Contents lists available at ScienceDirect

Physics Letters B

www.elsevier.com/locate/physletb

Polyakov loop potential at finite density

CrossMark

Christian S. Fischer [a], Leonard Fister [b], Jan Luecker [a,*], Jan M. Pawlowski [c,d]

[a] *Institut für Theoretische Physik, JLU Gießen, Heinrich-Buff-Ring 16, 35392 Gießen, Germany*
[b] *Department of Mathematical Physics, National University of Ireland Maynooth, Maynooth, County Kildare, Ireland*
[c] *Institut für Theoretische Physik, Universität Heidelberg, Philosophenweg 16, 69120 Heidelberg, Germany*
[d] *ExtreMe Matter Institute EMMI, GSI Helmholtzzentrum für Schwerionenforschung mbH, 64291 Darmstadt, Germany*

A R T I C L E   I N F O

A B S T R A C T

The Polyakov loop potential serves to distinguish between the confined hadronic and the deconfined quark–gluon plasma phases of QCD. For $N_f = 2 + 1$ quark flavors with physical masses we determine the Polyakov loop potential at finite temperature and density and extract the location of the deconfinement transition. We find a crossover at small values of the chemical potential running into a critical end-point at $\mu/T > 1$.

1. Introduction

In recent years much progress has been made in our understanding of the phase structure of QCD at finite temperature and density. This understanding has been achieved with a variety of methods ranging from first principle lattice and continuum computations to elaborate model studies.

At vanishing density all these methods by now converge quantitatively leaving only a few open fundamental questions, e.g. the order of the phase transitions in different regions of the Columbia plot. In turn, at finite density, progress has been hampered by several intricate problems. On the lattice one has to face the sign problem which so far has made it impossible to access chemical potentials with $\mu/T > 1$ [1,2]. First principle continuum computations with functional methods, such as Dyson–Schwinger equations (DSE) and functional renormalization group (FRG) equations, are based on an expansion of the theory in terms of quark–gluon correlation functions. Hence at finite density they have to cope with the increasingly complicated ground state structure of QCD in terms of these correlation functions. Finally, low energy effective models are usually anchored and benchmarked at the vacuum and thermal physics at vanishing density. In turn, the more important the density fluctuations get, the less quantitative are the results.

Facing these problems, it is apparent that progress in our understanding of QCD at finite temperature and density is probably best achieved by a combination of the different methods at hand. In the present work we push forward the functional continuum approach towards the phase diagram of QCD supplemented with results from lattice QCD. We determine, for the first time, the Polyakov loop potential at finite temperature and real chemical potential.

2. The phase diagram with functional methods

In the past decade continuum quark and gluon correlations functions have been computed with the help of functional equations for the effective action of QCD. These works have been mostly performed in (background) Landau gauge,

$$\bar{D}_\mu A_\mu = 0, \quad \text{with } \bar{D}_\mu = \partial_\mu - ig\bar{A}_\mu, \tag{1}$$

where $\bar{A}$ is chosen to be the expectation value of the gauge field, $\bar{A} = \langle A \rangle$. Note that correlation functions in ordinary Landau gauge are directly related to those in background Landau gauge by simply substituting plain momentum p^2 with background covariant momentum, $p^2 \to -\bar{D}^2$, for a detailed discussion see [3,4]. In this approach the Polyakov loop variable

$$L = \frac{1}{N_c} \text{tr}_{\text{fund}} P(\vec{x}), \quad \text{with } P(\vec{x}) = \mathcal{P} e^{\text{i}g \int_0^\beta dx_0 \, A_0(x_0, \vec{x})}, \tag{2}$$

in the fundamental representation, evaluated at the minimum of the Polyakov loop effective potential $V[A_0]$, is an order parameter for confinement in the heavy quark limit [3,5]. The effective potential is defined from the effective action Γ, evaluated at constant background fields A_0^{const} and vanishing gauge fields,

$$V[A_0^{\text{const}}] := \frac{1}{\beta \mathcal{V}} \Gamma[A_0^{\text{const}}; 0]. \tag{3}$$

* Corresponding author.

Fig. 1. DSE for the background gluon one-point function. Large circles indicate dressed propagators and vertices, and S stands for the classical action, see [4].

Fig. 2. Functional flow for the effective action of QCD. Crosses indicate insertions of the functional cut-off. The field ϕ combines quark, ghost and gluon fields.

The minimum of $V[A_0]$ singles out the expectation value of the gauge field in the background Landau gauge, $\langle A_0 \rangle$. The related order parameter satisfies

$$L\big[\langle A_0 \rangle\big] \geqslant \big\langle L[A_0] \big\rangle \tag{4}$$

within an appropriate (re)normalization of $\langle L[A_0] \rangle$, see [3–6]. This inequality holds true for both, Yang–Mills theory and fully dynamical QCD. In the presence of a phase transition both sides vanish at T_c and the inequality (4) is saturated below T_c. In turn, in the presence of a crossover we expect the crossover temperature computed from $L[\langle A_0 \rangle]$ to be lower than the one computed from $\langle L[A_0] \rangle$.

The effective potential, or its A_0-derivative, can be computed from the functional DSE and FRG equations, see Fig. 1 and Fig. 2, respectively. For the FRG this has been put forward in Yang–Mills theory, [3–6], and in QCD at finite temperature and imaginary chemical potential in [7]. There, the effective potential $V[A_0]$ is computed solely from the scale-dependent propagators. More recently, a similar computation of the Polyakov loop potential has also been performed in Coulomb gauge, [8,9]. Related lattice computations can be found in [10–13].

In turn, the DSE-formulation has been put forward in [4]. It is apparent from Fig. 1, that the effective potential $V[A_0]$ can be computed from the DSE once the ghost, gluon and quark propagators as well as the three-gluon vertex and ghost-gluon vertex are known. In the present work we utilize the observation in Ref. [4] that within an optimized renormalization scheme the two-loop terms in Fig. 1 are sub-leading at temperatures about T_c. This has been thoroughly tested for Yang–Mills theory within a comparison of the DSE results from Fig. 1 with the FRG results from Fig. 2. For temperatures about T_c the results agree quantitatively. The inclusion of the quark-loop in full QCD does not change this picture. Moreover, we neglect the A_0-dependence of the back-reaction of the Polyakov loop potential to the chromo-electric propagator in terms of $\partial_{A_0}^2 V[A_0]$. While these back-reaction effects may be crucial for the critical scaling of the chromo-electric component of the gluon propagator close to the phase transition of pure Yang–Mills theory [4,14], we expect its influence on the QCD transition to be small. This needs to be verified in future work.

Within this approximation the A_0-dependence solely originates from the shifted Matsubara frequencies $p_0 + gA_0$, and hence the propagator equations can be solved in Landau gauge. The diagrams in Fig. 1 and Fig. 2 can be diagonalized in color space leaving us with

$$p_0 + 2\pi T\varphi_m, \tag{5}$$

where φ_m are the eigenvalues of $\beta gA_0/(2\pi)$, depending on the representation. For example, for two-color QCD, the constant tem-

poral gauge field can be rotated into the Cartan subalgebra, $A_0 = 2\pi T\varphi/g\tau^3$, with Cartan generator τ^3. We have the eigenvalues

$$\varphi_{\mathrm{ad}} \in \{\pm\varphi, 0\}, \qquad \varphi_{\mathrm{fund}} \in \left\{\pm\frac{\varphi}{2}\right\}, \tag{6}$$

in the adjoint and fundamental representation respectively. The factors $1/2$ in φ_{fund} carry information on the explicit center-symmetry breaking of the quarks.

In the physical case of $SU(3)$ we restrict ourselves to $2\pi T\varphi/g\tau^3$ in the Cartan subalgebra generated by τ^3, τ^8.[1] The corresponding eigenvalues are given by

$$\varphi_{\mathrm{ad}} \in \left\{\pm\varphi, \pm\frac{\varphi}{2}, \pm\frac{\varphi}{2}, 0, 0\right\}, \qquad \varphi_{\mathrm{fund}} \in \left\{\pm\frac{\varphi}{2}, 0\right\}, \tag{7}$$

for more details see [4,6]. Then, the shifted Matsubara frequencies $p_0 + gA_0$ read after diagonalization,

$$2\pi T(n + \varphi_{\mathrm{ad}}), \quad \text{and} \quad 2\pi T\left(n + \frac{1}{2} + \varphi_{\mathrm{fund}}\right), \tag{8}$$

for ghost, gluon in the adjoint representation and the quark in the fundamental representation respectively. The additive nature of the loop representation in Fig. 1 and Fig. 2 leads to the simple form

$$V(\varphi) = V_{\mathrm{glue}}(\varphi) + V_{\mathrm{quark}}(\varphi). \tag{9}$$

Here, V_{glue}, contains all contributions from the gluon and ghost diagrams in the DSE and FRG, see Figs. 1, 2.

In the present approximation, i.e. without the back-reaction of $V[A_0]$ to the chromo-electric gluon (as detailed above), all diagrams contributing to V_{glue} involve only traces and contractions in the adjoint representation, and hence the eigenvalues φ_{ad} in (6), (7). In turn, the matter contribution, V_{quark}, involves only traces and contractions in the fundamental representation, and hence the eigenvalues φ_{fund} in (6), (7). With (8) this leads to the periodicities

$$V_{\mathrm{glue}}(\varphi + 2) = V_{\mathrm{glue}}(\varphi), \qquad V_{\mathrm{quark}}(\varphi + 2) = V_{\mathrm{quark}}(\varphi), \tag{10}$$

for the physical case of $SU(3)$. For comparison we also quote the $SU(2)$-case where we have

$$V_{\mathrm{glue}}(\varphi + 1) = V_{\mathrm{glue}}(\varphi), \qquad V_{\mathrm{quark}}(\varphi + 2) = V_{\mathrm{quark}}(\varphi). \tag{11}$$

We observe that the periodicity of V_{quark} is independent of N_c in contrast to that of the glue part. The latter dependence reflects the fact that V_{glue} is center-symmetric and hence invariant under Z_{N_c}-transformations. For the simple case of $N_c = 2$ the Cartan is one-dimensional and a center transformation entails $\varphi \to 1 - \varphi$ with center-symmetric point $\varphi = 1/2$. Evidently this is not the symmetry of the quark potential V_{quark} due to its periodicity, see (11). The Polyakov loop in the fundamental representation in $SU(2)$ reads

$$L(\varphi) = \cos(\pi\varphi), \tag{12}$$

and vanishes at the center-symmetric point $\varphi = 1/2$.

For $N_c = 3$ (and higher N_c) a center transformation is a rotation in the Cartan. Accordingly, the explicit center-breaking in the quark potential is only visible for general gauge fields in the Cartan sub-algebra, i.e., $A_0 = A_0^3\tau^3 + A_0^8\tau^8$, which are not considered here. Interestingly, for $SU(3)$ the quark potential has the same periodicity w.r.t. φ as the glue potential in contradistinction to $SU(2)$. This may be a helpful property for model applications at finite density, [15–22], and shall be studied elsewhere. The Polyakov loop in three-color QCD reads

$$L(\varphi) = \frac{1}{3}\big(1 + 2\cos(\pi\varphi)\big), \tag{13}$$

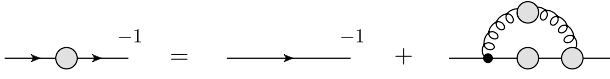[1] At finite chemical potential, this involves a center average.

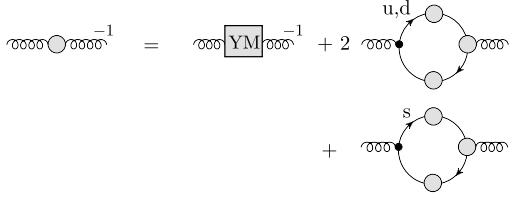**Fig. 3.** The DSE for the quark propagator.

Fig. 4. The truncated gluon DSE for $N_f = 2 + 1$ QCD. The first term is the inverse quenched propagator.

and vanishes at the confining values $\varphi = 2/3, 4/3$ in the fundamental period $\varphi \in \{0, 2\}$. This gives us direct access to an order parameter potential for the confinement–deconfinement phase transition in a DSE-approach to the phase structure of QCD as put forward in [23,24]. In the following we will exploit this approach at finite temperature and density thus providing first insights into the Polyakov loop potential at finite density.

3. DSE for the quark and gluon propagators

In order to determine the $N_f = 2 + 1$ quark and gluon propagators at finite temperature and chemical potential we have solved their corresponding DSEs given diagrammatically in Figs. 3 and 4. In the gluon DSE we work with an approximation neglecting unquenching effects in the Yang–Mills part of the equation. Consequently this part can be replaced by the inverse quenched propagator denoted by the diagram with the box labelled 'YM' in Fig. 4. This approximation is valid on the few percent level [24]. For the quenched gluon propagator one may use corresponding lattice results [14,26–28] or input from an FRG calculation within Yang–Mills theory [4,29]. We have checked that our results for the potential and the respective critical temperatures are hardly affected by this choice. This is a direct consequence of the inheritance of the above-mentioned renormalization scheme in the quenched case [4], allowed by the absence of two-loop diagrams in the matter sector of the DSE. To make contact with the results of Ref. [24] in the following we use the lattice results of Ref. [26] as input. The only other unknown quantity in our system of DSEs is the fully dressed quark–gluon vertex. Since no reliable calculations of this quantity at finite temperature are available, we resort to the model ansatz of Refs. [23,24]. There, the vertex is constructed utilizing information from the Slavnov–Taylor identity of the vertex as well as constraints due to the perturbative RG running of the vertex. It has been shown in [24] that such an ansatz is sufficient to deliver results for the chiral condensate at finite temperature in good agreement with lattice gauge theory [30]. A further justification of our quark–gluon interaction is given in Fig. 5. In the thermal medium, the color-diagonal gluon propagator is given by

$$D_{\mu\nu}(p) = P_{\mu\nu}^L(p) \frac{Z^L(p)}{p^2} + P_{\mu\nu}^T(p) \frac{Z^T(p)}{p^2}, \quad (14)$$

where the dressing functions Z^L and Z^T represent the parts with longitudinal and transversal orientation with respect to the heat bath and the $P_{\mu\nu}^{T,L}$ are the corresponding projectors. For three different temperatures these dressing functions are plotted in Fig. 5. The dashed lines are fits to the quenched lattice data of [26]. The unquenched results (solid lines), predicted in the DSE framework [24], are compared with very recent unquenched lattice results
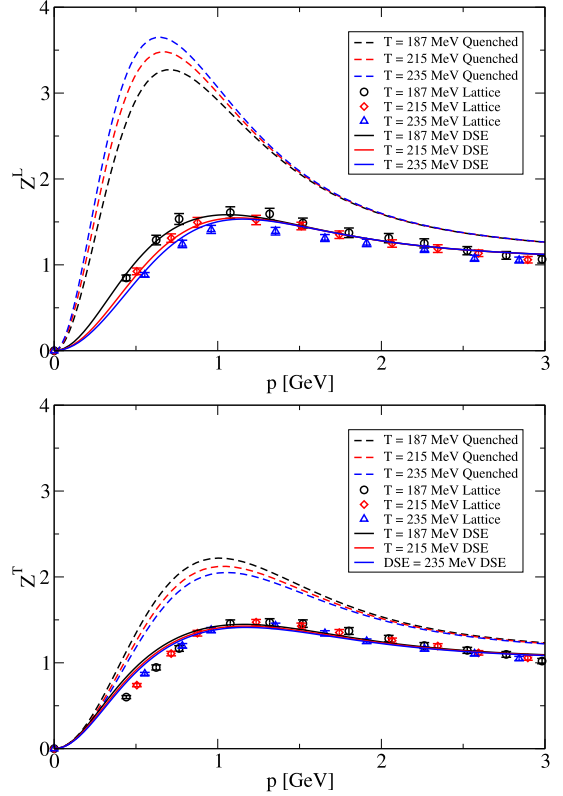

Fig. 5. Quenched and unquenched gluon dressing functions Z^L (upper plot) and Z^T (lower plot), see (14), compared to gauge-fixed unquenched lattice data from [25]. (For interpretation of colors in this figure, the reader is referred to the web version of this article.)

from Ref. [25]. We observe large unquenching effects in the longitudinal part of the propagator and somewhat smaller effects in the magnetic part. For both dressing functions the prediction from the functional framework is nicely matched by the lattice data. We believe these results provide solid justification for the vertex construction and the truncation of the gluon DSE used in our work.

To summarize the approximations made in our approach, we solve the quark and gluon DSEs in a truncation established in [26]. For the quark–gluon vertex we resort to a model *ansatz*. For the gluon we use a combination of lattice data and the fermionic vacuum polarization. With the resulting propagators, we solve the DSE for the background field, Fig. 1. By using an optimized renormalization scheme [4], we are able to minimize the corrections from two-loop terms, which we therefore neglect in our truncation. Furthermore, the A_0-dependence is only taken into account as a shift in the Matsubara modes, in accordance with the arguments from [4].

4. Results

The DSE for the potential depicted in Fig. 1 is used to compute $\partial_\varphi V(\varphi)$. Upon φ-integration this yields the Polyakov loop potential $V(\varphi)$ as a function of temperature and chemical potential. In Fig. 6 and Fig. 7 we show the dimensionless potential $V(\varphi)/p_{SB}$ with $V(0) = 0$ and $p_{SB} = \frac{19\pi^2}{36} T^4 + \frac{3}{2} T^2 \mu^2 + \frac{3}{4\pi^2} \mu^4$. The pressure is hidden in the integration constant [4] and will be discussed elsewhere.

We have computed the Polyakov loop potential $V(\varphi)$ in $2 + 1$ flavor QCD at the physical pion mass. In Yang–Mills theory, the confining minimum with vanishing Polyakov loop, $L(\varphi) = 0$, is at $\varphi = 2/3$, see (13). In turn, for $\varphi = 0$ one has $L(\varphi = 0) = 1$.

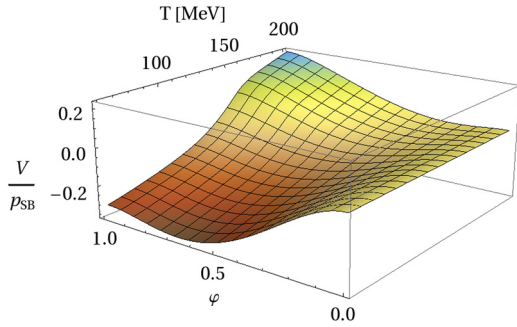**Fig. 6.** Polyakov loop potential defined in (3) for $\mu = 0$.
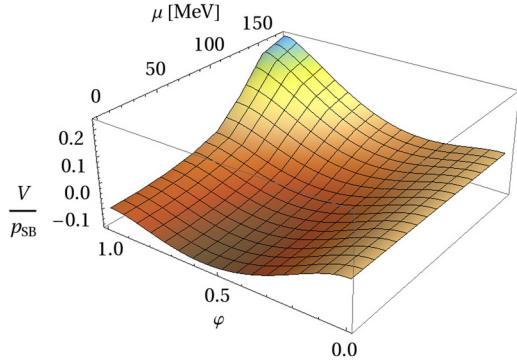

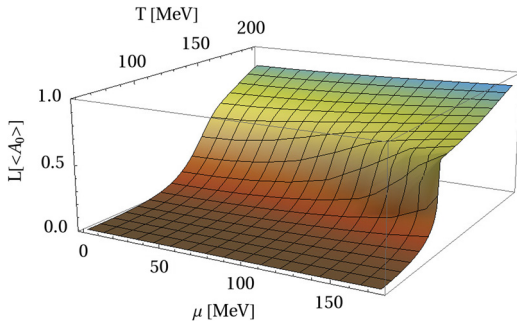**Fig. 7.** Polyakov loop potential for $T = 132$ MeV.

Fig. 8. Polyakov loop in the μ–T-plane.

Here, in $N_f = 2 + 1$ QCD this situation is approximately realized, thus reflecting the expected crossover behavior. Still, one clearly sees the transition from the confining regime at low temperature/small chemical potential to the deconfined phase at high temperature/large chemical potential. The sharper crossover transition as a function of chemical potential with fixed $T = 132$ MeV reflects the proximity of the critical endpoint.

Fig. 8 shows the Polyakov loop (2) evaluated at the minimum $\langle A_0 \rangle$ of the effective potential $V[A_0]$. For small chemical potential or densities the deconfinement transition is a smooth crossover. There is no unique definition of the crossover temperature T_{conf}. In the present work we use the inflection point of the Polyakov loop,

$$\partial_T L\big[\langle A_0 \rangle\big]\big|_{T_{conf}} \geqslant \partial_T L\big[\langle A_0 \rangle\big], \tag{15}$$

i.e., the maximum of the thermal derivative. Other definitions include the inflection point of the expectation value $\langle A_0 \rangle$, and that of the dual chiral condensate as computed in [24] for $2 + 1$ flavors. In [24] the crossover temperature is computed from the susceptibility and differs slightly from the dual T_{conf} computed here. Also the quark masses have been slightly larger than the physical ones;
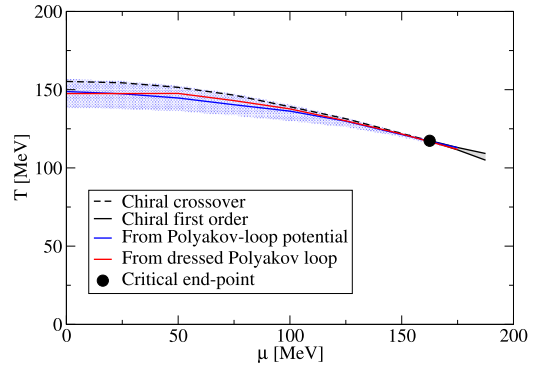

Fig. 9. Phase diagram for chiral symmetry restoration and deconfinement for $N_f = 2 + 1$. (For interpretation of colors in this figure, the reader is referred to the web version of this article.)

this has been corrected in the present work. The crossover sharpens with increasing chemical potential and finally turns into a first order transition at $(T_*, \mu_*) = (117 \text{ MeV}, 163 \text{ MeV})$. Note that the critical point (T_*, μ_*) as well as the first order line does not depend on the definition of the crossover temperature. In Fig. 9 we show T_{conf} together with the chiral transition temperature T_χ which is obtained from the inflection point of the light-quark condensate. The shaded area shows the width of the deconfinement crossover defined by 80% of the inflection peak. Interestingly, all transition temperatures, T_{conf} and T_χ agree within this width for the whole phase diagram. Since definitions of T_{conf} with either Polyakov loop potential or dressed Polyakov loop are based on different properties of the quark and gluon correlation functions, this provides a highly non-trivial check of the self-consistency of the present approximation. Nevertheless, at very large chemical potential the present scheme may not be sufficient, see Ref. [24] for a more detailed discussion.

In this work we presented the first results for the Polyakov loop potential at finite chemical potential in QCD with $N_f = 2 + 1$, evaluated from a combination of functional and lattice methods. Our results provide input for model calculations, see e.g. [22]. Although several approximations are involved (as detailed above) we are confident that we have provided qualitatively reliable results that may serve as a guide for future evaluations of the potential with different methods. The minimum of the potential provides an order parameter that is accessible solely from the propagators of QCD, and yields a deconfinement temperature that is, consistently with that of the dressed Polyakov loop, in vicinity of the chiral transition.

Acknowledgements

References

[1] G. Endrodi, Z. Fodor, S. Katz, K. Szabo, J. High Energy Phys. 1104 (2011) 001, arXiv:1102.1356 [hep-lat].
[2] O. Kaczmarek, F. Karsch, E. Laermann, C. Miao, S. Mukherjee, et al., Phys. Rev. D 83 (2011) 014504, arXiv:1011.3130 [hep-lat].
[3] J. Braun, H. Gies, J.M. Pawlowski, Phys. Lett. B 684 (2010) 262, arXiv:0708.2413 [hep-th].

[4] L. Fister, J.M. Pawlowski, Phys. Rev. D 88 (2013) 045010, arXiv:1301.4163 [hep-ph].

[5] F. Marhauser, J.M. Pawlowski, arXiv:0812.1144 [hep-ph], 2008.

[6] J. Braun, A. Eichhorn, H. Gies, J.M. Pawlowski, Eur. Phys. J. C 70 (2010) 689, arXiv:1007.2619 [hep-ph].

[7] J. Braun, L.M. Haas, F. Marhauser, J.M. Pawlowski, Phys. Rev. Lett. 106 (2011) 022002, arXiv:0908.0008 [hep-ph].

[8] H. Reinhardt, J. Heffner, Phys. Lett. B 718 (2012) 672, arXiv:1210.1742 [hep-th].

[9] H. Reinhardt, J. Heffner, Phys. Rev. D 88 (2013) 045024, arXiv:1304.2980 [hep-th].

[10] J. Langelage, S. Lottini, O. Philipsen, J. High Energy Phys. 1102 (2011) 057, arXiv:1010.0951 [hep-lat].

[11] D. Diakonov, C. Gattringer, H.-P. Schadler, J. High Energy Phys. 1208 (2012) 128, arXiv:1205.4768 [hep-lat].

[12] J. Greensite, Phys. Rev. D 86 (2012) 114507, arXiv:1209.5697 [hep-lat].

[13] J. Greensite, K. Langfeld, Phys. Rev. D 87 (2013) 094501, arXiv:1301.4977 [hep-lat].

[14] A. Maas, J.M. Pawlowski, L. von Smekal, D. Spielmann, Phys. Rev. D 85 (2012) 034037, arXiv:1110.6340 [hep-lat].

[15] R.D. Pisarski, Phys. Rev. D 62 (2000) 111501, arXiv:hep-ph/0006205.

[16] A. Dumitru, Y. Hatta, J. Lenaghan, K. Orginos, R.D. Pisarski, Phys. Rev. D 70 (2004) 034511, arXiv:hep-th/0311223.

[17] T.K. Herbst, J.M. Pawlowski, B.-J. Schaefer, Phys. Lett. B 696 (2011) 58, arXiv:1008.0081 [hep-ph].

[18] V. Skokov, B. Friman, K. Redlich, Phys. Rev. C 83 (2011) 054904, arXiv:1008.4570 [hep-ph].

[19] W. Weise, Prog. Part. Nucl. Phys. 67 (2012) 299, arXiv:1201.0950 [nucl-th].

[20] N.M. Bratovic, T. Hatsuda, W. Weise, Phys. Lett. B 719 (2013) 131, arXiv:1204.3788 [hep-ph].

[21] K. Fukushima, K. Kashiwa, Phys. Lett. B 723 (2013) 360, arXiv:1206.0685 [hep-ph].

[22] L.M. Haas, R. Stiele, J. Braun, J.M. Pawlowski, J. Schaffner-Bielich, Phys. Rev. D 87 (2013) 076004, arXiv:1302.1993 [hep-ph].

[23] C.S. Fischer, J. Luecker, J.A. Mueller, Phys. Lett. B 702 (2011) 438, arXiv:1104.1564 [hep-ph].

[24] C.S. Fischer, J. Luecker, Phys. Lett. B 718 (2013) 1036, arXiv:1206.5191 [hep-ph].

[25] R. Aouane, F. Burger, E.-M. Ilgenfritz, M. Müller-Preussker, A. Sternbeck, Phys. Rev. D 87 (2013) 114502, arXiv:1212.1102 [hep-lat].

[26] C.S. Fischer, A. Maas, J.A. Muller, Eur. Phys. J. C 68 (2010) 165, arXiv:1003.1960 [hep-ph].

[27] R. Aouane, V.G. Bornyakov, E.-M. Ilgenfritz, V.K. Mitrjushkin, M. Müller-Preussker, A. Sternbeck, Phys. Rev. D 85 (2012) 034501.

[28] A. Cucchieri, T. Mendes, PoS LATTICE2011 (2011) 206, arXiv:1201.6086 [hep-lat].

[29] L. Fister, J.M. Pawlowski, arXiv:1112.5440 [hep-ph], 2011.

[30] S. Borsanyi, et al., Wuppertal-Budapest Collaboration, QCD phase transition, J. High Energy Phys. 1009 (2010) 073, arXiv:1005.3508 [hep-lat].